
This is an electronic reprint of the original article.
This reprint may differ from the original in pagination and typographic detail.

Österlund, Elmeri; Kinnunen, Jere; Rontu, Ville; Torkkeli, Altti; Paulasto-Kröckel, Mervi
Mechanical properties and reliability of aluminum nitride thin films

Published in:
Journal of Alloys and Compounds

DOI:
[10.1016/j.jallcom.2018.09.062](https://doi.org/10.1016/j.jallcom.2018.09.062)

Published: 25/01/2019

Document Version
Peer-reviewed accepted author manuscript, also known as Final accepted manuscript or Post-print

Published under the following license:
CC BY-NC-ND

Please cite the original version:
Österlund, E., Kinnunen, J., Rontu, V., Torkkeli, A., & Paulasto-Kröckel, M. (2019). Mechanical properties and reliability of aluminum nitride thin films. *Journal of Alloys and Compounds*, 772, 306-313.
<https://doi.org/10.1016/j.jallcom.2018.09.062>

This material is protected by copyright and other intellectual property rights, and duplication or sale of all or part of any of the repository collections is not permitted, except that material may be duplicated by you for your research use or educational purposes in electronic or print form. You must obtain permission for any other use. Electronic or print copies may not be offered, whether for sale or otherwise to anyone who is not an authorised user.

Mechanical Properties and Reliability of Aluminum Nitride Thin Films

Elmeri Österlund^{a,*}, Jere Kinnunen^a, Ville Rontu^b, Altti Torkkeli^c, Mervi Paulasto-Kröckel^a

^a*Aalto University, Department of Electrical Engineering and Automation, PO Box 13500, 00076 Aalto, Finland*

^b*Aalto University, Department of Chemistry and Materials Science, PO Box 13500, 00076 Aalto, Finland*

^c*Murata Electronics Oy, Myllynkivenkuja 6, 01621 Vantaa, Finland*

Abstract

Knowledge of the mechanical properties and fatigue behavior of thin films is important for the design and reliability of microfabricated devices. This study uses the bulge test to measure the residual stress, Young's modulus, and fracture strength of aluminum nitride (AlN) thin films with different microstructures prepared by sputtering, metalorganic vapor phase epitaxy (MOVPE), and atomic layer deposition (ALD). In addition, the fatigue behavior is studied under cyclic loading. The results indicate that the fracture strength and Young's modulus of AlN are mainly determined by the film microstructure, which is consecutively influenced by the deposition method and conditions. A microstructure with a higher order of crystallinity has increased fracture strength and Young's modulus. Additionally, the strength limiting defects are located at the film-substrate interface. The measured residual stresses were 249, 876, 1,526, and 272 MPa for two sputtered films

*Corresponding author

Email address: elmeri.osterlund@aalto.fi (Elmeri Österlund)

of different thicknesses, MOVPE and ALD films, respectively. The fracture strengths were 1.42, 1.54, 2.76, and 0.61 GPa, and Young's moduli were 335, 343, 346, and 272 GPa. No clear signs of fatigue were observed after 10,000 cycles at a load corresponding to 83% of the fracture strength.

Keywords: Mechanical properties, Nitride materials, Thin films, Microstructure

1. Introduction

Aluminum nitride (AlN) is a piezoelectric wide band gap high temperature III-V compound with many possible applications. For example, AlN thin films are used or show potential in microelectromechanical systems (MEMS) such as bulk acoustic wave (BAW) [1] and thin film bulk acoustic resonators (FBAR) [2], energy harvesters [3], inertial sensors [4], and microphones [5]. In optoelectronics, AlN thin films can be used for instance in deep ultraviolet devices [6–9]. The electrical and piezoelectric properties of AlN are already relatively well known [10, 11], due to the widespread and established use in these applications.

However, despite the tremendous interest in AlN, the mechanical properties, which are a crucial part of the operation and reliability of microfabricated devices [12, 13], of thin film AlN are not fully known. Out of the important mechanical properties, i.e. fracture strength, Young's modulus, and fatigue behavior, only Young's modulus has been studied. The previous studies have mainly used nanoindentation in determining Young's modulus and this has led to lower than expected results. Previously, *ab initio* calculations [14, 15], Brillouin light scattering [16, 17], and ultrasonic methods [18]

have been used as well.

20 All the previous studies have given a very wide range for Young's modulus ranging from 204 GPa [19] to 396 GPa [15], due to the differences in the test methods and tested films. Moreover, the fatigue behavior or the fracture strength of thin film AlN, and their effects on reliability have not been studied previously. So far, these gaps in knowledge have hindered the commercial
25 utilization of AlN, especially in piezoelectric MEMS devices.

Certainly, a need exists for more accurate determination of Young's moduli and the other mechanical properties of AlN thin films, and it should be clarified what causes the differences in measured Young's moduli. For reliable and accurate characterization of the mechanical properties, the test method
30 needs to be selected carefully. Several different micro- and nanomechanical testing methods have been used previously. These include methods such as the aforementioned nanoindentation [19–21], as well as microbending [22, 23], microcompression [24, 25] and microtensile testing [22, 26], and shaft loading [27].

35 Especially for thin and stiff films such as AlN, estimating mechanical properties by the above methods is difficult. Nanoindentation suffers for example from the substrate effect, film cracking and phase changes [19, 28]. In microbending, dislocations accumulate at the neutral plane changing the mechanical behavior [29]. Microcompression testing has its own pitfalls, including FIB-induced damage, the taper of the pillars, difficulty in aligning
40 the setup and uncalibrated loading conditions [29]. Microtensile testing eliminates some of these problems but requires a significant amount of work in sample preparation.

In comparison, the bulge test method [27, 30] is simpler and does not suffer from the same drawbacks. This method requires no careful alignment of the measurement setup and the throughput of the sample fabrication process is considerably better. Furthermore, the original stress state of the film is retained, and the test gives an accurate estimate of the residual stresses as well. Additionally, there are no stringent requirements for the film thickness, as in microcompression or nanoindentation. As a result, films can be tested at the application-relevant length scale, which influences the mechanical properties of thin films [29].

This study uses the bulge test to measure the fracture strength, Young's modulus, and residual stress of AlN thin films deposited on silicon substrates using three different deposition methods. Furthermore, the fatigue behavior is studied as well. In order to advance the understanding between the mechanical properties and microstructure, the films are characterized using X-ray diffraction (XRD). It is not known how the microstructure and deposition method affect the mechanical properties, especially the fracture strength. Generally, high deposition temperatures lead to high-quality films with fewer flaws and better microstructures [31]. The hypothesis tested in this study is that films with better microstructures are stronger and behave more reliably. In order to test this, AlN films with different microstructures are produced using reactive sputtering, metalorganic vapor phase epitaxy (MOVPE), and atomic layer deposition (ALD).

2. Experimental

2.1. AlN Deposition

AlN films were deposited using sputtering, MOVPE and ALD. The sputtered films were grown using pulsed DC reactive sputtering. Al target (99.9999%
70 purity) was sputtered under 10 sccm of Ar and 50 sccm of N₂ flows after a base pressure of less than 130 μ Pa was reached. The total pressure was 333 mPa and the power used was 6 kW at 100 kHz and 60% duty cycle. Target thicknesses for the films were 50 and 200 nm. (111) Si wafers 100 mm in diameter and 450 μ m thick were used as the substrates.

75 The MOVPE film was grown in an Aixtron close-coupled showerhead reactor using a three-step process with pre-growth, low-temperature buffer, and main growth steps. The low-temperature buffer layer has been shown to increase the film quality [32, 33]. First, in the pre-growth step, the substrate was cleaned and primed by baking it at 1 025 °C for 5 minutes under 30
80 kPa H₂ atmosphere and for 10 minutes under silane (SiH₄) flow of 50 sccm. Then the substrate was primed for AlN growth by nitridation of the surface under ammonia (NH₃) flow of 15 sccm and pressure of 10 kPa for 15 s at 980 °C. Before the main AlN growth step, the low-temperature AlN buffer layer was grown for 3 min at 980 °C using trimethylaluminum (TMAI, C₃H₉Al)
85 and NH₃ as precursors with flows of 336 sccm and 56 sccm, respectively. The reactor pressure was 67.6 kPa, and the resulting V/III ratio was 337. Finally, the AlN layer was grown at a substrate temperature of 1 085 °C for 15 minutes. Otherwise, the process parameters were the same as for the low-temperature layer. A 150 mm diameter 950 μ m thick (111) Si wafer was
90 used as the substrate.

ALD (Picosun SUNALE R-200 Advanced) was used to deposit a low-stress AlN film. The plasma-enhanced (PEALD) process used aluminum trichloride (AlCl_3) and NH_3 as precursors at a temperature of 425 °C. In ALD, the precursors are introduced into the reaction chamber in pulses one
95 at a time and the chamber is purged with an inert gas between the pulses. This results in a self-terminating layer-by-layer growth. The full process used to grow the ALD film is presented in a previous study [34]. The substrate was a 390 μm thick 150 mm diameter (100) Si wafer.

2.2. Sample Fabrication

100 After AlN deposition, the bulge test samples were fabricated using through wafer etching of silicon, as shown in Fig. 1a. First, an Al_2O_3 hard mask was grown on the backside of the wafers using thermal ALD (Beneq TFS-500), with TMAI and H_2O precursors at a temperature of 220 °C. Thicknesses of the Al_2O_3 layers were 53 nm, 124 nm, and 50 nm for sputtered, MOVPE, and
105 ALD samples, respectively. The mask was patterned using photolithography (Süss MA-6, AZ 5214E photoresist, AZ 351B developer) and wet etching (a mixture of H_3PO_4 and HNO_3 at 50 °C). The lithography mask used in this step defined the chip size ($7 \times 7 \text{ mm}^2$) and the diameter of the circular membranes (900 μm). The membrane diameter for the thinner ALD samples
110 was 200 μm . The actual diameters were measured later. Then after resist removal, the substrates were attached to a carrier wafer using photoresist in order to protect the AlN film on the front side and to hold the chips in place. The wafers were etched from the backside using a deep reactive ion etching (DRIE) Bosch process with SF_6 and O_2 etch gases and C_4F_8 passivation
115 (STS advanced silicon etcher). Because the AlN layer acts as an etch-stop,

this process results in samples with free-standing AlN membranes. The etch process used has a high selectivity between Al₂O₃ and Si [35], and a low etch rate for AlN [36]. After DRIE, the samples were released and cleaned in acetone and isopropanol baths.

120 The samples used for fracture strength measurement required no additional processing. The samples used in the estimation of residual stress and Young's modulus were attached to polydimethylsiloxane (PDMS) blocks (Fig. 1b) in order to create a pressure seal between the sample and the tester. First, PDMS was cured at 50 °C and then cut into blocks with a hole
125 punched in the middle. Then the test samples were attached to the blocks with additional PDMS and cured again.

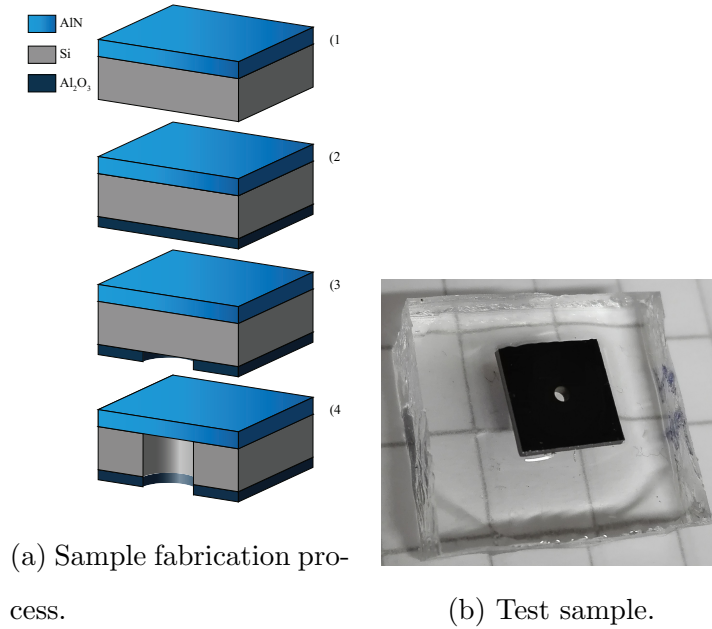


Figure 1: (a) Sample fabrication: 1) AlN deposition by either sputtering, MOVPE or ALD, 2) ALD Al₂O₃ etch mask on the backside, 3) lithography and wet etching of Al₂O₃ in a solution of H₃PO₄ and HNO₃, 4) DRIE of silicon to create free-standing circular AlN membranes. (b) A bulge test sample attached to a PDMS block used for testing.

2.3. Bulge Test

Bulge testing (Fig. 2) was used to measure the residual stress, Young's modulus and fracture strength of the films. The maximum deflection at the center of the membrane was measured as a function of pressure using a bulge tester with a Mirau-type scanning white light interferometer (SWLI) [37]. The sample was clamped to a holder, and the cavity was pressurized with argon gas. The pressure was increased by hand using a pressure regulator (Aga 600B 7P) and measured with an external gauge (Huber Instrumente HM35) attached to the line. From the measured pressure-deflection curves,

it was possible to determine the residual stress and Young's modulus of each measured sample. The external gauge used was considerably more accurate than just the gauge of the pressure regulator used in a previous study [27].

The fracture strength could be determined from the pressure alone, and
140 these measurements were done with a different bulge tester without a SWLI
after determining the residual stress and Young's modulus of the films. In-
stead, the second tester had automatic pressure control, and it could ac-
curately detect at which pressure the membrane fractured, with a nominal
accuracy of 100 Pa. The pressure ramp rate was also controllable and was 1
145 kPa/s in the fracture strength measurements. The fatigue cycling was also
done using this setup.

It was assumed that no plastic deformation occurs in the AlN membranes
and that the elastic deformation was linear until fracture. In other words, it
was assumed that the films behaved according to linear-elastic fracture me-
150 chanics (LEFM). For AlN thin films, this should be a reasonable assumption.
The bulge test should result in a mostly tensile stress state in the deflected
membrane and result in mode I (opening) fractures.

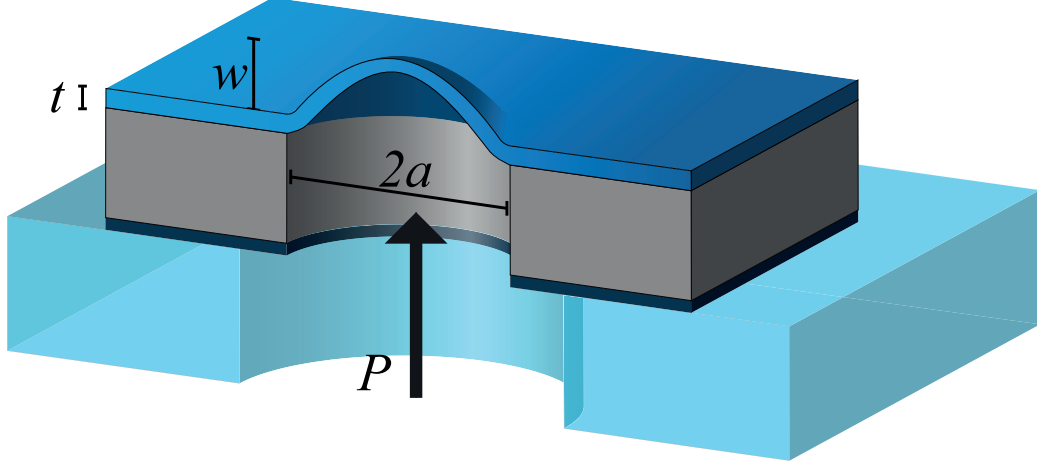


Figure 2: Schematic of the bulge test setup. Adapted from [27]. The fracture strength samples did not require a PDMS block and the pressure seal was created simply with an O-ring.

Young's modulus E and residual stress σ_0 were determined from the pressure-deflection measurements by fitting them in least squares sense into the following equation, which gives the pressure $P(w)$ in the cavity as a function of the membrane deflection w as

$$P(w) = c_1 \frac{t\sigma_0}{a^2} w + c_2 \frac{tE}{a^4(1-\nu)} w^3, \quad (1)$$

where c_1 and c_2 are constants depending on the geometry, t is the thickness of the film, a is the radius of the membrane, and ν is Poisson's ratio [38].

155 For circular membranes, FEM simulations [39] give the constants as $c_1 = 4$ and $c_2 = 2.67(1.026 + 0.233\nu)^{-1}$. The measured Poisson's ratio for AlN thin films ranges from 0.177 to 0.255 [40]. A value of 0.207 was used in this study for Poisson's ratio [41].

The fracture strength σ_f at the fracture pressure P_f , when residual stress is taken into account [42], is

$$\sigma_f^3 - \sigma_0 \sigma_f^2 - \frac{1}{24} \frac{EP_f^2 a^2}{(1-\nu)t^2} = 0 \quad (2)$$

By using the residual stress and Young's modulus previously determined for the films from the pressure-deflection measurements, it is possible to derive the fracture strength of the samples from the fracture pressures by finding the real root of Eq. (2).

2.4. Film Characterization

The deposited AlN films were characterized using optical and scanning electron microscopy (SEM), ellipsometry, and X-ray diffraction (XRD). The thicknesses of the films were measured after deposition with a Plasmos SD2300 ellipsometer. The actual diameter of each membrane was determined by imaging them with an Olympus BX51M optical microscope equipped with a Leica DFC420 digital camera. The diameter was measured from these images using image processing software.

The crystal- and microstructure of the films were characterized using XRD. Wide area χ - 2θ 2D diffraction maps were measured using a Rigaku SmartLab X-ray diffractometer equipped with a 9 kW rotating Cu anode source and a 2D single photon counting pixel detector HyPix-3000.

3. Results

The wide area χ - 2θ 2D diffraction maps are presented in Fig. 3 for the sputtered (Figs. 3a and 3b), MOVPE (Fig. 3c) and ALD (Fig. 3d) films. The measured reflections are labeled according to database references

[43]. The 2θ full widths at half maximum (FWHM) of the 002 reflections
180 were approximately 0.42° , 0.37° , and 0.35° , for the 55 nm sputtered, 220 nm
sputtered and 126 nm MOVPE films, respectively. For the ALD film, the
intensity of the 002 reflection was too low for a meaningful estimation of the
FWHM.

The results show that the sputtered and MOVPE films are textured with
185 preferential orientation of the c -axis. The width of the AlN002 reflection
indicates that the MOVPE film has the highest crystallinity compared to the
other films. The ALD film is not as crystalline and untextured in comparison.
The XRD results show that the MOVPE film, which was deposited at the
highest temperature, has the best crystal quality and orientation of the polar
190 c -axis. The AlN002 reflection is very narrow and strong compared to the
other films. The 002 reflection is also present in the sputtered films. However,
it is wider in both χ and 2θ directions, indicating that the orientation of the
grains is more spread and that the grains are also smaller. In the ALD film,
the 002 reflection is the weakest and is spread over a wide χ -range.

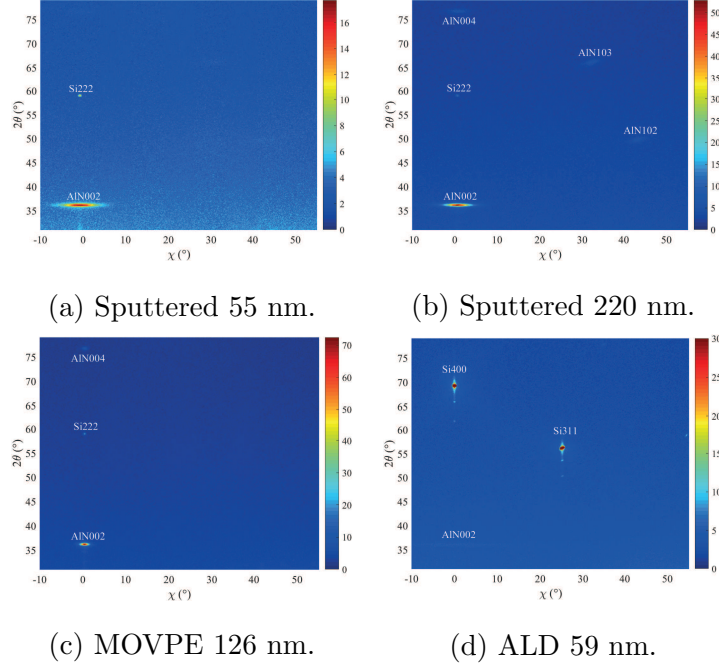


Figure 3: Measured χ - 2θ 2D diffraction maps for all AlN thin films.

195 The maximum deflections of the AlN membranes were measured as a function of pressure, with the SWLI setup from three to five samples per film. One example of a deflection measurement is presented in Fig. 4. The results were fitted into Eq. (1) in a least squares sense, as shown in Fig. 5. The calculated residual stresses and Young's moduli are presented in Table

200 1.

The mechanical strength of the films was determined by pressurizing 30 samples per film to fracture. The probability of fracture P_f is given by the Weibull distribution [44–46] as

$$P_f = 1 - e^{-A \left(\frac{\sigma - \sigma_{th}}{\sigma'} \right)^m}, \quad (3)$$

where σ is the multiaxial stress in the specimen with a surface area of A , σ_{th} is the threshold stress below which no fracture occurs, σ' is the characteristic stress (63% probability of fracture), and m is the Weibull modulus. The threshold stress can be assumed to be zero for brittle materials [47]. Instead of the surface area A , sample volume V should be used if the fractures are caused by volume defects instead of surface ones. The Weibull probability of fracture vs. fracture strength distributions for the measured films are presented in Fig. 6. The average fracture strengths are presented in Table 1. No adhesion failures between the substrate and the film were observed in optical microscopy after testing.

The wafer curvature method [48] gives the average residual stresses of the films as 212 MPa, 738 MPa, 1.8 GPa, and 165 MPa for the sputtered (55 and 122 nm), MOVPE and ALD films, respectively.

Table 1: Thickness, membrane diameter, residual stress, Young’s modulus and fracture strength of different AlN thin film membranes.

| Deposition method | Thickness (nm) | Membrane diameter (μm) | Residual stress (MPa) | Young’s modulus (GPa) | Strength (GPa) |
|-------------------|-----------------|-------------------------------------|-----------------------|-----------------------|-----------------|
| Sputtering | 54.9 ± 0.6 | 957 ± 20 | 249 ± 63 | 335 ± 3 | 1.42 ± 0.46 |
| Sputtering | 220.0 ± 2.3 | 973 ± 7.0 | 876 ± 78 | 343 ± 8 | 1.54 ± 0.18 |
| MOVPE | 126.0 ± 5.2 | $1\ 014 \pm 2.1$ | $1\ 526 \pm 100$ | 346 ± 43 | 2.76 ± 0.34 |
| ALD | 58.6 ± 0.7 | 252 ± 14 | 272 ± 58 | 257 ± 102 | 0.61 ± 0.10 |

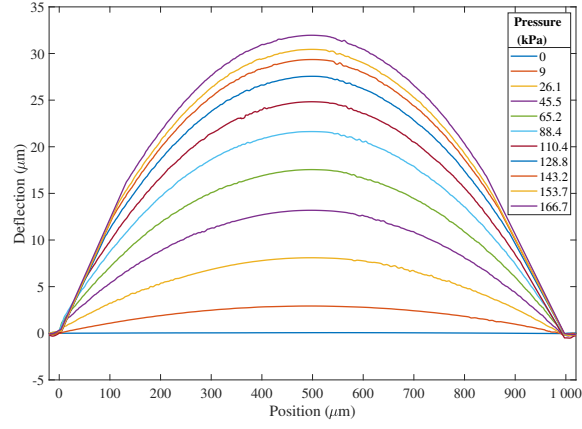


Figure 4: Deflection of a MOVPE deposited AlN thin film membrane along the diameter as a function of position at different pressures.

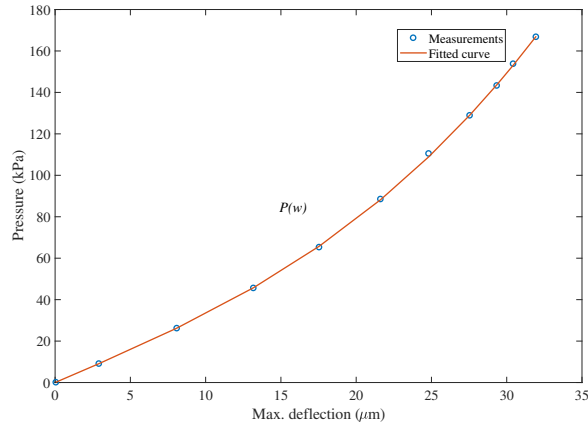


Figure 5: Pressure vs. maximum membrane deflection measurements for the sample in Fig. 4 with a curve fitted according to Eq. (1) giving estimates for the residual stress and Young's modulus.

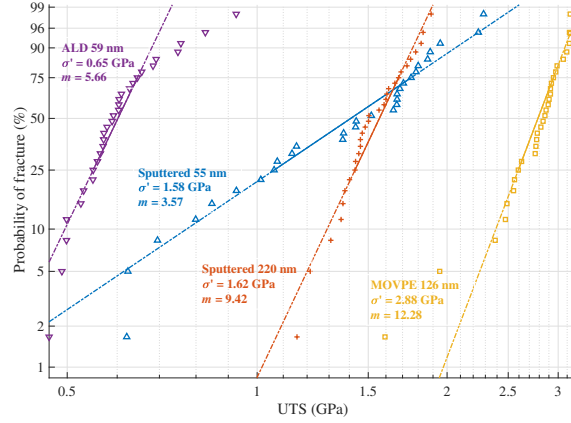


Figure 6: Weibull distributions of the fracture strengths of the sputter, MOVPE, and ALD deposited AlN thin films. The points were calculated from the experimental data using Eq. (2).

3.1. Fatigue

The fatigue of AlN was studied by cycling the 220 nm thick sputtered film for 10,000 cycles at a load of approximately 83% of the measured average fracture strength. The mechanical stress profile used in fatigue cycling as a function of time is presented in Figure 7. Loading of 83% was selected in order to induce possible fatigue as fast as possible, while still keeping a significant amount of samples intact. The residual stress, Young's modulus, and fracture strength were measured using the previously described methods, with the exception of a smaller sample size of 20 for the fracture strength measurement. The results are presented in Table 2, and the Weibull distributions are presented in Fig. 8. The changes in the residual stress and Young's modulus were statistically compared to the uncycled film using Student's t -test and the probability (p) for a no statistically significant change

230 is presented in Table 2 as well. Three samples fractured in the first cycle during fatigue testing.

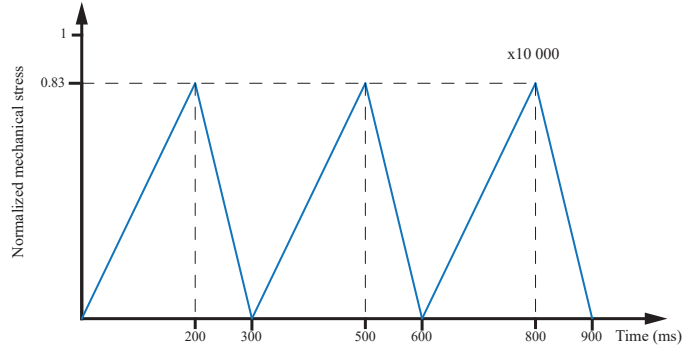


Figure 7: The mechanical stress profile as a function of time used in the fatigue cycling of AlN films.

Table 2: Residual stress, Young’s modulus, and fracture strength of 220 nm thick sputtered AlN film before and after mechanical cycling. The p -value indicates the probability that no statistically significant changes occurred according to the t -test.

| Film | Residual stress (MPa) | Young’s modulus (GPa) | Fracture strength (GPa) |
|--------------|--------------------------|--------------------------|----------------------------|
| As-deposited | 879.03 ± 74.02 | 342.58 ± 7.07 | 1.54 ± 0.18 |
| Fatigued | 950.79 ± 71.20 | 337.25 ± 10.70 | 1.52 ± 0.11 |
| p -value | 0.24 | 0.50 | |

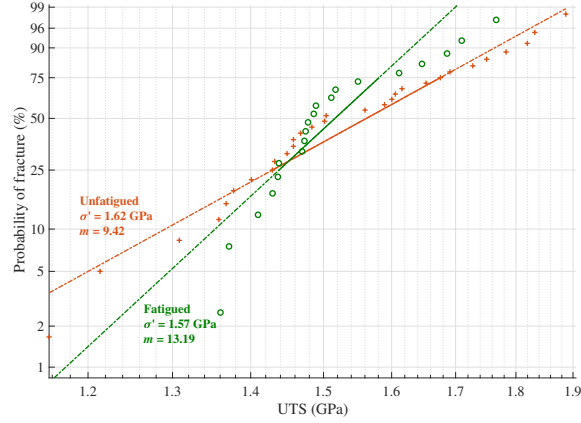


Figure 8: Weibull distributions of the fracture strength of as-deposited and fatigued 220 nm thick sputtered samples.

4. Discussion

Compared to the previously reported experimental measurements for Young’s modulus of AlN thin films, the results presented here are notably higher and closer to the calculated values. The reported values in the literature for Young’s modulus are between 204 and 396 GPa [15, 19]. The wide range is due to differences in the test methods and in the tested films. For example, the most used method, nanoindentation testing, gives values lower than expected due to the substrate effect. Moreover, the indentation depth affects the measured value, even when testing the same film with the same tester, reducing Young’s modulus from 277 to 204 GPa in one case [19]. *Ab initio* calculations and Brillouin light scattering (BLS) have yielded noticeably higher values. The calculated Young’s moduli ranged from 237 to 353 GPa [14, 15] and BLS measured from 291–321 GPa [16] to 351 GPa [17] for sputtered and bulk AlN, respectively.

In addition to the different testing methods, the wide range of values is caused by differences in the tested films. A correlation has been observed in some cases between the crystallinity and mechanical properties [49]. For single crystalline bulk AlN, Young's modulus can be as high as 374 GPa [41]. For polycrystalline bulk and thin film AlN, values of 320 [18] and 300 GPa [50], respectively, have been reported. And for amorphous AlN, Young's moduli are between 66 [51] and 200 GPa [49].

There seems to be a similar correlation between the observed crystallinity and Young's moduli of the films tested in this study. The ALD film, which has the lowest crystallinity, also has the lowest measured Young's modulus at 257 GPa. Although, the deviation in the results is quite large (± 102 GPa). The MOVPE and sputtered films have very similar measured moduli, despite the MOVPE film being slightly more crystalline (AlN 002 FWHM 0.35° vs. 0.42° and 0.37°). Young's moduli of the MOVPE and sputtered films are between what has been reported for single crystalline and polycrystalline films, whereas the modulus of the ALD film is between polycrystalline and amorphous. The fracture strengths of the three types of film varied considerably more and correlate with the observed crystallinity.

In theory, the fracture strength of thin films should decrease with increasing film thickness because a larger volume will contain more flaws if they are uniformly distributed. The average fracture strength of the sputtered films did not change noticeably between the 55 and 220 nm thick films. Because the fracture strength of a material is mainly determined by its fracture toughness in combination with the size and distribution of flaws [52], the results indicate that the flaw distribution did not change as the thickness increased.

This suggests that the defects dominating the fracture strength are mainly located at the interface between the film and the substrate. Another explanation is that flaws caused by sample fabrication limit the fracture strength. Moreover, the testing method used could potentially change the failure mode of the membranes. In theory, the failures should initiate near the center of the membrane, where the strain is greatest. The membrane fractures could also be caused by poor adhesion between the film and substrate around the membrane or by fractures initiated near the substrate-membrane interface. However, using optical microscopy, no fractures were observed caused by loss of adhesion or by fracture initiation around the membrane circumference.

The deposition methods used in this study are ones commonly used to deposit AlN thin films. Of these, reactive sputtering is perhaps the most used method and generally results in moderately high-quality polycrystalline and textured films with moderate stresses [53, 54]. Possible defects include argon incorporation and damage from ion bombardment [55]. MOVPE growth typically results in very high quality and purity films [32, 56]. However, the film stresses are also high due to high growth temperatures and coefficient of thermal expansion (CTE) mismatch between substrate and film. ALD AlN films are usually polycrystalline and can include a high amount of impurities from the process gases [57, 58]. However, ALD is a popular deposition method due to low growth temperatures, accurate thickness control, and uniformity as well as good conformal coverage on high aspect ratio structures [59]. The fracture strength results for the sputtered, MOVPE and ALD films confirm that the MOVPE film had the highest quality, followed by sputtered and ALD films.

The residual stresses acquired with the bulge method probably provide a more accurate estimate compared to substrate curvature measurements. The bulge test is a more direct method in comparison, and it includes fewer assumptions about the materials. In addition, the effect of the substrate is minimized compared to the curvature method, while the film is still clamped to the substrate at the edges, retaining its original stress state. Moreover, wafer curvature gives the average stress over the whole wafer, whereas it is possible to accurately map the residual stress over the wafer using the bulge test.

The two main causes of residual stress in as-deposited films are the CTE and lattice mismatches between the substrate and the film [60, 61]. The lattice mismatch is 0.23 between AlN and Si. Clearly, an elastic strain of 23% is not feasible, and most of the lattice mismatch is accommodated. The CTE misfit strain is $1.80 \cdot 10^{-3}$ and $0.68 \cdot 10^{-3}$ for the MOVPE and ALD films, respectively, using CTE values of $5.3 \cdot 10^{-6}/\text{K}$ for AlN and $3.6 \cdot 10^{-6}/\text{K}$ for Si [62] and assuming that the CTEs are constant over the temperature range. The corresponding residual stresses are 786 and 221 MPa for the MOVPE and ALD film, respectively, using the measured Young's moduli.

The fatigue testing of the 220 nm thick sputtered film shows no statistically significant changes in the residual stress or Young's modulus after 10,000 cycles at 83% load of the measured fracture strength. As the residual stress did in fact slightly increase, this could indicate that there were no symptoms of fatigue that cause a relaxation of stresses, such as plastic flow, creep, or microcracking. Furthermore, sub-critical crack growth or propagation of microcracks should have been noticeable in the average fracture

strength. The strength of the fatigued samples does not seem to follow the Weibull distribution as well and shows a decrease when the stress is higher than 1.5 GPa. The Weibull modulus at high stress matches the modulus of the unfatigued samples more closely. The slightly higher Weibull modulus
325 of the fatigued samples is likely because the mechanically weakest samples were already eliminated during fatigue cycling.

Interestingly, the Weibull distribution of the ALD film shows two populations. The Weibull modulus decreases at high stress, and the modulus at stresses above 0.6 GPa in the ALD film resembles the modulus for the 55
330 nm sputtered film. No change is apparent in the 220 nm sputtered or in the MOVPE film.

Based on the Weibull modulus, the films can be divided into two categories: high and low modulus films. The MOVPE and 220 nm sputtered films and the low-stress part of the ALD belong to the high modulus category, whereas the 55 nm sputtered and the high-stress part of the ALD film
335 belong to the low category. The presence of the two categories indicates that there could be two failure modes that cause the fractures. The two modes are most likely caused by the inherent material flaws and flaws generated by the sample fabrication. In theory, the flaws in the high category are more evenly
340 distributed in the film and from sample to sample and cause less variance in the results. In the low category, the flaws are unevenly distributed and clustered, which means that these films can be considered unreliable. Most likely, the fractures in the high category films are caused by the inherent material flaws, thus these results represent the actual strength of the material.

345 The MOVPE and 220 nm thick sputtered films can be considered strong

and reliable. Between the 55 nm and 220 nm thick sputtered films, the only difference is the Weibull moduli. Films below the 100 nm range behave less reliably, and the failure mode is different. ALD film has a considerable Weibull modulus despite being 58 nm thin, which seems to indicate that the
350 ALD film is uniform yet mechanically weak.

Typical materials used with AlN include Si, Pt, Mo, Ti, and Al. Si has a measured mechanical strength of 1.5–7.2 GPa [63], while metals typically have strengths in the 100 MPa range. In light of this, the results show that AlN films deposited by sputtering or MOVPE are mechanically stronger and
355 should not pose a problem for device reliability. AlN films deposited with ALD require more consideration in their use.

The factors that contributed to the error in the results and their estimated size or measured standard deviation were as follows: Assumption of Poisson’s ratio (± 0.039), accuracy of the pressure measurement (± 1 kPa),
360 measurement uncertainty of the SWLI (± 20 nm), film thickness variation (± 1 , ± 2.3 , ± 5.2 , and ± 0.8 nm for 55, 220 nm sputtered, MOVPE, and ALD), change of the film thickness due to over-etching (-1 nm), and measurement error in the bulge radius (± 20 , ± 10 , ± 35 and ± 14 μm).

5. Conclusion

365 In this study, the bulge test method was used to investigate the mechanical properties of AlN thin films prepared by sputtering, metalorganic vapor phase epitaxy (MOVPE) and atomic layer deposition (ALD). The residual stress, Young’s modulus, and fracture strength were measured for all three films. In addition, the fatigue of AlN was studied by measuring the possible

370 changes to the mechanical properties of the film due to cyclic stress. The
microstructures of the films were investigated using XRD.

The results show that the fracture strength of AlN thin films depends on
the microstructure of the film, which is determined by the deposition method.
Films deposited at higher temperatures have higher crystal quality and are
375 mechanically stronger. From a reliability point of view, the associated higher
residual stresses somewhat offset this increase in strength. Young's modulus
depends on the crystallinity of the film up to a point. The results presented
in this study differ from the previous experimental values and are closer to
the actual Young's modulus of AlN.

380 No substantial effects of fatigue were observed in the sputter deposited
AlN film. The mechanical properties of the film did not change significantly
after 10,000 loading cycles. However, the Weibull distribution of the fracture
strength changed slightly, indicating that cyclic loading might cause some
changes in AlN thin films. Fatigue in AlN thin films was studied for the first
385 time using the bulge test method.

This study shows that AlN is a mechanically strong and reliable material,
suitable to be used in MEMS and in other micro- and nanoscale devices. Of
the used deposition methods, sputtering and MOVPE are appropriate when
high strength is required and residual stresses are not an issue. ALD is best
390 suited to be used when properties of the film other than mechanical are more
important for the application.

Acknowledgments

The authors acknowledge Mr. Keiichi Umeda and Mr. Yasuhiro Aida from Murata Manufacturing, Dr. Sami Suihkonen and Mr. Jori Lemettinen
395 from Aalto University, and Mr. Anton Nolvi, Prof. Edward Hægström, Dr. Ivan Kassamakov and Mr. Jouni Heino from the University of Helsinki. Most of the research was performed at the OtaNano - Micronova Nanofabrication Centre and Nanomicroscopy Center. This research was supported by the ECSEL2014-2-662155 project: Informed, NPI grant of the European
400 Space Agency, and donation made by Murata Electronics Oy. Mr. Rontu is thankful for funding by the Finnish Cultural Foundation.

References

- [1] R. Jakkuraju, G. Henn, C. Shearer, M. Harris, N. Rimmer, P. Rich, Integrated Approach to Electrode and AlN Depositions for Bulk Acoustic Wave (BAW) Devices, *Microelectron. Eng.* 70 (2-4) (2003) 566–570. doi:10.1016/s0167-9317(03)00386-1.
405
- [2] K.-W. Tay, C.-L. Huang, L. Wu, Highly c-axis oriented thin AlN films deposited on gold seed layer for FBAR devices, *J. Vac. Sci. Technol. B* 23 (4) (2005) 1474–1479. doi:10.1116/1.1941249.
- [3] M. Renaud, K. Karakaya, T. Sterken, P. Fiorini, C. Van Hoof, R. Puers, Fabrication, modelling and characterization of MEMS piezoelectric vibration harvesters, *Sensor. Actuat. A-phys.* 145 (2008) 380–386. doi:10.1016/j.sna.2007.11.005.
410

- 415 [4] S. Trolier-McKinstry, P. Muralt, Thin film piezoelectrics for MEMS, *J. Electroceram.* 12 (1) (2004) 7–17. doi:10.1007/0-387-23319-9_10.
- [5] M. D. Williams, B. A. Griffin, T. N. Reagan, J. R. Underbrink, M. Sheplak, An AlN MEMS piezoelectric microphone for aeroacoustic applications, *J. Microelectromech. S.* 21 (2) (2012) 270–283. doi:10.1109/jmems.2011.2176921.
- 420 [6] P. Chen, R. Zhang, Z. Zhao, D. Xi, B. Shen, Z. Chen, Y. Zhou, S. Xie, W. Lu, Y. Zheng, Growth of high quality GaN layers with AlN buffer on Si (111) substrates, *J. Cryst. Growth* 225 (2) (2001) 150–154. doi:10.1016/s0022-0248(01)00842-9.
- 425 [7] A. Krost, A. Dadgar, GaN-based optoelectronics on silicon substrates, *Mater. Sci. Eng. B-adv.* 93 (1) (2002) 77–84. doi:10.1016/s0921-5107(02)00043-0.
- [8] S. Qu, S. Li, Y. Peng, X. Zhu, X. Hu, C. Wang, X. Chen, Y. Gao, X. Xu, Influence of the growth temperature of AlN buffer on the quality and stress of GaN films grown on 6H-SiC substrate by MOVPE, *J. Alloys Compd.* 502 (2) (2010) 417–422. doi:10.1016/j.jallcom.2010.04.185.
- 430 [9] J.-T. Oh, Y.-T. Moon, J.-H. Jang, J.-H. Eum, Y.-J. Sung, S. Y. Lee, J.-O. Song, T.-Y. Seong, High-performance GaN-based light emitting diodes grown on 8-inch Si substrate by using a combined low-temperature and high-temperature-grown AlN buffer layer, *J. Alloys Compd.* 732 (2018) 630–636. doi:10.1016/j.jallcom.2017.10.200.

- [10] M.-A. Dubois, P. Muralt, Stress and piezoelectric properties of aluminum nitride thin films deposited onto metal electrodes by pulsed direct current reactive sputtering, *J. Appl. Phys.* 89 (11) (2001) 6389–6395. doi:10.1063/1.1359162.
- [11] R. E. Newnham, *Properties of Materials: Anisotropy, Symmetry, Structure*, Oxford University Press, Oxford, 2005. doi:10.5860/choice.42-6504.
- [12] S. Allameh, An introduction to mechanical-properties-related issues in MEMS structures, *J. Mater. Sci.* 38 (20) (2003) 4115–4123. doi:10.1023/A:1026369320215.
- [13] W. M. Van Spengen, MEMS reliability from a failure mechanisms perspective, *Microelectron. Reliab.* 43 (7) (2003) 1049–1060. doi:10.1016/s0026-2714(03)00119-7.
- [14] E. Ruiz, S. Alvarez, P. Alemany, Electronic structure and properties of AlN, *Phys. Rev. B* 49 (11) (1994) 7115. doi:10.1103/physrevb.49.7115.
- [15] A. Wright, Elastic properties of zinc-blende and wurtzite AlN, GaN, and InN, *J. Appl. Phys.* 82 (6) (1997) 2833–2839. doi:10.1063/1.366114.
- [16] G. Carlotti, G. Gubbiotti, F. Hickernell, H. Liaw, G. Socino, Comparative study of the elastic properties of polycrystalline aluminum nitride films on silicon by Brillouin light scattering, *Thin Solid Films* 310 (1-2) (1997) 34–38. doi:10.1016/s0040-6090(97)00343-x.

- [17] M. Kazan, E. Moussaed, R. Nader, P. Masri, Elastic constants of aluminum nitride, *Phys. Status Solidi C* 4 (1) (2007) 204–207. doi: 460 10.1002/pssc.200673503.
- [18] S. Dodd, G. Saunders, M. Cankurtaran, B. James, Ultrasonic study of the elastic and nonlinear acoustic properties of ceramic aluminum nitride, *J. Mater. Sci.* 36 (3) (2001) 723–729. doi:10.1023/A: 465 1004897126648.
- [19] M. Reusch, S. Cherneva, Y. Lu, A. Žukauskaitė, L. Kirste, K. Holc, M. Datcheva, D. Stoychev, V. Lebedev, O. Ambacher, Microstructure and mechanical properties of stress-tailored piezoelectric AlN thin films for electro-acoustic devices, *Appl. Surf. Sci.* 407 (2017) 307–314. doi: 470 10.1016/j.apsusc.2017.02.147.
- [20] D. T. Read, A. A. Volinsky, Measurements for Mechanical Reliability of Thin Films, in: *Nato. Sci. Peace. Secur.*, Springer, 2009, pp. 337–358. doi:10.1007/978-90-481-2792-4_16.
- [21] V. Moraes, H. Riedl, R. Rachbauer, S. Kolozsvári, M. Ikeda, 475 L. Prochaska, S. Paschen, P. Mayrhofer, Thermal conductivity and mechanical properties of AlN-based thin films, *J. Appl. Phys.* 119 (22) (2016) 225304. doi:10.1063/1.4953358.
- [22] M. Haque, M. Saif, A review of MEMS-based microscale and nanoscale tensile and bending testing, *Exp. Mech.* 43 (3) (2003) 248–255. doi: 480 10.1177/0014485103036018.

- [23] C. Motz, T. Schöberl, R. Pippan, Mechanical properties of micro-sized copper bending beams machined by the focused ion beam technique, *Acta Mater.* 53 (15) (2005) 4269–4279. doi:10.1016/j.actamat.2005.05.036.
- 485 [24] M. D. Uchic, D. M. Dimiduk, J. N. Florando, W. D. Nix, Sample dimensions influence strength and crystal plasticity, *Science* 305 (5686) (2004) 986–989. doi:10.1126/science.1098993.
- [25] P. J. Imrich, C. Kirchlechner, D. Kiener, G. Dehm, In situ TEM micro-compression of single and bicrystalline samples: insights and limitations,
490 *JOM* 67 (8) (2015) 1704–1712. doi:10.1007/s11837-015-1440-6.
- [26] D. Kiener, W. Grosinger, G. Dehm, R. Pippan, A further step towards an understanding of size-dependent crystal plasticity: In situ tension experiments of miniaturized single-crystal copper samples, *Acta Mater.* 56 (3) (2008) 580–592. doi:10.1016/j.actamat.2007.10.015.
- 495 [27] M. Berdova, T. Ylitalo, I. Kassamakov, J. Heino, P. T. Törmä, L. Kilpi, H. Ronkainen, J. Koskinen, E. Hægström, S. Franssila, Mechanical assessment of suspended ALD thin films by bulge and shaft-loading techniques, *Acta Mater.* 66 (2014) 370–377. doi:10.1016/j.actamat.2013.11.024.
- 500 [28] R. Saha, W. D. Nix, Effects of the substrate on the determination of thin film mechanical properties by nanoindentation, *Acta Mater.* 50 (1) (2002) 23–38. doi:10.1016/s1359-6454(01)00328-7.

- [29] G. Dehm, B. Jaya, R. Raghavan, C. Kirchlechner, Overview on Micro- and Nanomechanical Testing: New Insights in Interface Plasticity and Fracture at Small Length Scales, *Acta Mater.* doi:10.1016/j.actamat.2017.06.019.
- [30] F. Knöbber, V. Züribig, N. Heidrich, J. Hees, R. E. Sah, M. Baeumler, S. Leopold, D. Pätz, O. Ambacher, V. Lebedev, Static and dynamic characterization of AlN and nanocrystalline diamond membranes, *Phys. Status Solidi A* 209 (10) (2012) 1835–1842. doi:10.1002/pssa.201228180.
- [31] J. A. Thornton, The microstructure of sputter-deposited coatings, *J. Vac. Sci. Technol. A* 4 (6) (1986) 3059–3065. doi:10.1116/1.573628.
- [32] W. Luo, L. Li, Z. Li, Q. Yang, D. Zhang, X. Dong, D. Peng, L. Pan, C. Li, B. Liu, et al., Influence of the nucleation layer morphology on the structural property of AlN films grown on c-plane sapphire by MOCVD, *J. Alloys Compd.* 697 (2017) 262–267. doi:10.1016/j.jallcom.2016.12.126.
- [33] F. Malengreau, S. Hagege, R. Sporken, M. Vermeersch, R. Caudano, UHV reactive sputtering of AlN (0001) single crystals on Si (111) at high temperature by a two-step growth method, *J. Eur. Ceram. Soc.* 17 (15-16) (1997) 1807–1811. doi:10.1016/s0955-2219(97)00073-3.
- [34] V. Rontu, P. Sippola, M. Broas, G. Ross, T. Sajavaara, H. Lipsanen, M. Paulasto-Kröckel, S. Franssila, Atomic layer deposition of AlN from

- 525 AlCl₃ using NH₃ and Ar/NH₃ plasma, *J. Vac. Sci. Technol. A* 36 (2) (2018) 021508. doi:10.1116/1.5003381.
- [35] L. Sainiemi, S. Franssila, Mask material effects in cryogenic deep reactive ion etching, *J. Vac. Sci. Technol. B* 25 (3) (2007) 801–807. doi:10.1116/1.2734157.
- 530 [36] A. Perros, M. Bosund, T. Sajavaara, M. Laitinen, L. Sainiemi, T. Huh-
tio, H. Lipsanen, Plasma etch characteristics of aluminum nitride mask
layers grown by low-temperature plasma enhanced atomic layer deposi-
tion in SF₆ based plasmas, *J. Vac. Sci. Technol. A* 30 (1) (2012) 011504.
doi:10.1116/1.3664306.
- 535 [37] I. V. Kassamakov, H. O. Seppänen, M. J. Oinonen, E. O. Hægström,
J. M. Österberg, J. P. Aaltonen, H. Saarikko, Z. P. Radivojevic, Scan-
ning white light interferometry in quality control of single-point tape
automated bonding, *Microelectron. Eng.* 84 (1) (2007) 114–123. doi:
10.1016/j.mee.2006.08.013.
- 540 [38] J. Vlassak, W. Nix, A new bulge test technique for the determination of
Young’s modulus and Poisson’s ratio of thin films, *J. Mater. Res.* 7 (12)
(1992) 3242–3249. doi:10.1557/jmr.1992.3242.
- [39] J. Y. Pan, P. Lin, F. Maseeh, S. D. Senturia, Verification of FEM analysis
of load-deflection methods for measuring mechanical properties of thin
545 films, in: *Solid-State Sensor and Actuator Workshop, 1990. 4th Techni-
cal Digest., IEEE, IEEE, 1990*, pp. 70–73. doi:10.1109/solsen.1990.
109823.

- [40] M. Moram, M. Vickers, X-ray diffraction of III-nitrides, *Rep. Prog. Phys.* 72 (3) (2009) 036502. doi:10.1088/0034-4885/72/3/036502.
- 550 [41] I. Yonenaga, T. Shima, M. H. Sluiter, Nano-indentation hardness and elastic moduli of bulk single-crystal AlN, *Jpn. J. Appl. Phys.* 41 (7R) (2002) 4620. doi:10.1143/jjap.41.4620.
- [42] V. Rontu, A. Nolvi, A. Hokkanen, E. Haeggstroem, I. Kassamakov, S. Franssila, Elastic and fracture properties of free-standing amorphous ALD Al₂O₃ thin films measured with bulge test, *Mater. Res. Express*doi:10.1088/2053-1591/aabbd5.
- 555
- [43] G. Bergerhoff, I. Brown, F. Allen, et al., *Crystallographic databases*, International Union of Crystallography, Chester 360 (1987) 77–95.
- [44] W. Weibull, The phenomenon of rupture in solids, *J. of Appl. Mech.* 18
560 (1951) 293.
- [45] S. Greek, F. Ericson, S. Johansson, J.-Å. Schweitz, In situ tensile strength measurement and Weibull analysis of thick film and thin film micromachined polysilicon structures, *Thin Solid Films* 292 (1) (1997) 247 – 254. doi:10.1016/s0040-6090(96)09076-1.
- 565 [46] O. Borrero-López, M. Hoffman, A. Bendavid, P. J. Martin, Reverse size effect in the fracture strength of brittle thin films, *Scr. Mater.* 60 (11) (2009) 937 – 940. doi:10.1016/j.scriptamat.2009.01.042.
- [47] C. Lu, R. Danzer, F. D. Fischer, Influence of threshold stress on the estimation of the Weibull statistics, *J. Am. Ceram. Soc.* 85 (6) (2002) 1640–1642. doi:10.1111/j.1151-2916.2002.tb00330.x.
- 570

- [48] G. Janssen, M. Abdalla, F. Van Keulen, B. Pujada, B. Van Venrooy, Celebrating the 100th anniversary of the Stoney equation for film stress: Developments from polycrystalline steel strips to single crystal silicon wafers, *Thin Solid Films* 517 (6) (2009) 1858–1867. doi:10.1016/j.tsf.2008.07.014.
- 575
- [49] J. T. Gaskins, P. E. Hopkins, D. R. Merrill, S. R. Bauers, E. Hadland, D. C. Johnson, D. Koh, J. H. Yum, S. Banerjee, B. J. Nordell, et al., Investigation and Review of the Thermal, Mechanical, Electrical, Optical, and Structural Properties of Atomic Layer Deposited High-*k* Dielectrics: Beryllium Oxide, Aluminum Oxide, Hafnium Oxide, and Aluminum Nitride, *ECS J. Solid State Sci. Technol.* 6 (10) (2017) N189–N208. doi:10.1149/2.0091710jss.
- 580
- [50] V. Mortet, M. Nesladek, K. Haenen, A. Morel, M. D’Olieslaeger, M. Vanecek, Physical properties of polycrystalline aluminium nitride films deposited by magnetron sputtering, *Diamond Relat. Mater.* 13 (4–8) (2004) 1120–1124. doi:10.1016/j.diamond.2003.10.082.
- 585
- [51] B. Ilic, S. Krylov, H. Craighead, Youngs modulus and density measurements of thin atomic layer deposited films using resonant nanomechanics, *J. Appl. Phys.* 108 (4) (2010) 044317. doi:10.1063/1.3474987.
- [52] S. Zhang, D. Sun, Y. Fu, H. Du, Toughness measurement of thin films: a critical review, *Surf. Coat. Technol.* 198 (1) (2005) 74–84. doi:10.1016/j.surfcoat.2004.10.021.
- 590

- [53] M. A. Herman, W. Richter, H. Sitter, *Epitaxy: Physical Principles and Technical Implementation*, Springer, Berlin, 2004.
- 595 [54] G. Ke, Y. Tao, Y. Lu, Y. Bian, T. Zhu, H. Guo, Y. Chen, Highly c-axis oriented aln film grown by unbalanced magnetron reactive sputtering and its electrical properties, *J. Alloys Compd.* 646 (2015) 446–453. doi:10.1016/j.jallcom.2015.05.174.
- [55] H. F. Winters, E. Kay, Gas incorporation into sputtered films, *J. Appl. Phys.* 38 (10) (1967) 3928–3934. doi:10.1063/1.1709043.
- 600 [56] A. Dadgar, A. Krost, J. Christen, B. Bastek, F. Bertram, A. Krtschil, T. Hempel, J. Bläsing, U. Haboek, A. Hoffmann, MOVPE growth of high-quality AlN, *J. Cryst. Growth* 297 (2) (2006) 306–310. doi:10.1016/j.jcrysgr.2006.09.046.
- 605 [57] N. Nepal, S. Qadri, J. Hite, N. Mahadik, M. Mastro, C. Eddy Jr, Epitaxial Growth of AlN Films via Plasma-Assisted Atomic Layer Epitaxy, *Appl. Phys. Lett.* 103 (8) (2013) 082110. doi:10.1063/1.4818792.
- [58] M. Broas, P. Sippola, T. Sajavaara, V. Vuorinen, A. Pymaki Perros, H. Lipsanen, M. Paulasto-Kröckel, Structural and chemical analysis of annealed plasma-enhanced atomic layer deposition aluminum nitride films, *J. Vac. Sci. Technol. A* 34 (4) (2016) 041506. doi:10.1116/1.4953029.
- 610 [59] M. Knaut, M. Junige, V. Neumann, H. Wojcik, T. Henke, C. Hossbach, A. Hiess, M. Albert, J. W. Bartha, Atomic layer deposition for high

- 615 aspect ratio through silicon vias, *Microelectron. Eng.* 107 (2013) 80–83.
doi:10.1016/j.mee.2013.01.031.
- [60] R. Koch, The intrinsic stress of polycrystalline and epitaxial thin metal films, *J. Phys-condens. Mat.* 6 (45) (1994) 9519. doi:10.1088/0953-8984/6/45/005.
- 620 [61] L. B. Freund, S. Suresh, *Thin film materials: stress, defect formation and surface evolution*, Cambridge University Press, 2004. doi:10.1017/cbo9780511754715.
- [62] W. Yim, R. Paff, Thermal expansion of AlN, sapphire, and silicon, *J. Appl. Phys.* 45 (3) (1974) 1456–1457. doi:10.1063/1.1663432.
- 625 [63] F. Ericson, J.-Å. Schweitz, Micromechanical fracture strength of silicon, *J. Appl. Phys.* 68 (11) (1990) 5840–5844. doi:10.1063/1.346957.